Fate of inhaled monoclonal antibodies after the deposition of aerosolized particles in the respiratory system

Laurent Guilleminault, Nicolas Azzopardi, Christophe Arnoult, Julien Sobilo, Virginie Hervé, Jérôme Montharu, Antoine Guillon, Christian R. Andres, Olivier Hérault, Alain Le Pape, et al.

Fate of inhaled monoclonal antibodies after the deposition of aerosolized particles in the respiratory system

L. Guilleminault [a,b,c], N. Azzopardi [d], C. Arnoult [d], J. Sobilo [e], V. Hervé [b,f,g], J. Montharu [h], A. Guillon [b,f,g,i], C. Andres [j], O. Herault [k], A. Le Pape [e], P. Diot [a,b,c], E. Lemarié [a,b,c], G. Paintaud [d,l], V. Gouilleux-Gruart [d,m], N. Heuzé-Vourc'h [a,b,*]

[a] *Université François Rabelais, EA6305, F-37032 Tours, France*
[b] *Centre d'Etude des Pathologies Respiratoires, UMR 1100/EA6305, F-37032 Tours, France*
[c] *CHRU de Tours, Service de Pneumologie et d'Explorations Fonctionnelles, Tours, France*
[d] *Université François-Rabelais de Tours, CNRS, GICC UMR 7292, Tours, France*
[e] *TAAM-UPS44, CIPA, CNRS Orléans, Orléans, France*
[f] *Université François Rabelais, UMR 1100, F-37032 Tours, France*
[g] *INSERM, UMR 1100, F-37032 Tours, France*
[h] *Université François Rabelais de Tours, Faculté de Médecine, PPF Animalerie, Tours, France*
[i] *CHRU de Tours, Service de Réanimation Polyvalente, Tours, France*
[j] *CHRU de Tours, Service de Biochimie, Tours, France*
[k] *CHRU de Tours, Service d'Hématologie Biologique, Tours, France*
[l] *CHRU de Tours, Laboratory of Pharmacology-Toxicology, Tours, France*
[m] *CHRU de Tours, Laboratory of Immunology-Toxicology, Tours, France*

Monoclonal antibodies (mAbs) are usually delivered systemically, but only a small proportion of the drug reaches the lung after intravenous injection. The inhalation route is an attractive alternative for the local delivery of mAbs to treat lung diseases, potentially improving tissue concentration and exposure to the drug while limiting passage into the bloodstream and adverse effects. Several studies have shown that the delivery of mAbs or mAb-derived biopharmaceuticals *via* the airways is feasible and efficient, but little is known about the fate of inhaled mAbs after the deposition of aerosolized particles in the respiratory system. We used cetuximab, an anti-EGFR antibody, as our study model and showed that, after its delivery *via* the airways, this mAb accumulated rapidly in normal and cancerous tissues in the lung, at concentrations twice those achieved after intravenous delivery, for early time points. The spatial distribution of cetuximab within the tumor was heterogeneous, as reported after i.v. in-jection. Pharmacokinetic (PK) analyses were carried out in both mice and macaques and showed aerosolized cetuximab bioavailability to be lower and elimination times shorter in macaques than in mice. Using transgenic mice, we showed that FcRn, a key receptor involved in mAb distribution and PK, was likely to make a greater con-tribution to cetuximab recycling than to the transcytosis of this mAb in the airways. Our results indicate that the inhalation route is potentially useful for the treatment of both acute and chronic lung diseases, to boost and en-sure the sustained accumulation of mAbs within the lungs, while limiting their passage into the bloodstream.

1. Introduction

In recent decades biopharmaceuticals, such as monoclonal antibodies (mAb) and antibody-based biotherapeutic agents in particular, have become established major components in the therapeutic arsenal directed against cancers, and autoimmune and inflammatory diseases [1–3]. More than 30 mAbs or antibody-based biopharmaceuticals have been approved for sale around the world, for the treatment of various human diseases. Three mAbs (omalizumab, Xolair™; bevacizumab, Avastin™; palivizumab, Synagis™) are currently on the market for respiratory diseases, but another nine are currently in Phase III clinical trials [4]. Chronic lung diseases, such as lung cancer, chronic obstructive pulmonary disease (COPD), and idiopathic pulmonary fibrosis (IPF), thus continue to represent an unmet medical need with high morbidity and mortality [5–7].

The systemic route is generally used for the administration of mAbs in humans, resulting in very low concentrations of mAb in the lungs [8,9]. Moreover, this route exposes healthy organs to these potentially deleterious drugs and is associated with potential toxicity and severe

* Corresponding author at: CEPR, INSERM U1100/EA 6305, Faculté de Médecine, 10 Blvd. Tonnellé, F-37037 Tours Cedex, France. Tel.: +33 2 47 36 62 37; fax: +33 2 47 36 60 46.
E-mail address: nathalie.vourch@med.univ-tours.fr (N. Heuzé-Vourc'h).

adverse effects, such as a thickening of the serum and cytokine release syndrome [10]. Finally, systemic delivery is invasive, resulting in more frequent hospitalization of patients with chronic diseases, for at least short periods, for treatment. This increases clinical costs and limits patient compliance.

Most of the drugs in clinical trials for the treatment of lung diseases operate principally in the lungs (the organ housing the diseased tissue) rather than in the periphery. The direct targeting of the affected organ is thus an attractive option, to increase the therapeutic benefit of treatment while reducing the likelihood of adverse effects. The inhalation route is already widely used by clinicians for the administration of conventional chemical drugs and its tolerance profile is good [11]. This route is currently the accepted standard route for key respiratory drugs for COPD and asthma [12,13]. New opportunities for the use of this route have recently emerged, with the development of aerosolized antibiotics for the treatment of ventilator-acquired pneumonia with higher doses than can be administered systemically, due to safety concerns [14,15]. With the exception of dornasealfa (Pulmozyme®), a recombinant human DNase used to treat cystic fibrosis, the airways are used principally for the delivery of small drugs (beta2-adrenoreceptor agonists, muscarinic antagonists, and corticosteroids) [12,13]. We and others have shown that mAbs are resistant to the physical constraints of aerosolization, retaining their physical and immunological properties [16,17]. We have also shown that the airway route is potentially appropriate for the delivery of aerosolized cetuximab, an anti-EGFR monoclonal antibody, limiting the growth of tumors engrafted in the lungs while only very small amounts passing very slowly into the bloodstream [17]. Similarly, others reported the feasibility of delivering mAbs or antibody fragments through the airways to treat respiratory diseases such as respiratory infection, asthma and toxin-associated lung defect [18–20]. In contrast, inhaled omalizumab, an anti-IgE antibody, did not attenuate the early and late phase response to an inhaled allergen in a broncho-provocation model of asthma in humans [21]. However, the fact that inhaled mAbs passed poorly into the systemic circulation may provide a good rationale for the apparent lack of efficacy of inhaled-omalizumab. Indeed, omalizumab acts by reducing free IgE in the periphery and expression of FCεRI, thereby reducing the amount of IgE binding to mast cells, basophils, and eosinophils in the lung [22] . Presently, several questions remain to be answered before the transfer of this novel route of mAb delivery from the bench into the practice of respiratory care medicine. We explored the fate of cetuximab, used as a model mAb in this study on the basis of our knowledge of its behavior during aerosolization, after the deposition of aerosol particles in the lungs, in various animal models and with various imaging methods. We investigated the amount of cetuximab deposited on its target in the lungs, and the cellular distribution of this mAb in the normal and tumor tissues, in a mouse model of lung tumors expressing the target antigen. We also evaluated the effect of this treatment on the antitumor response. We then analyzed the pharmacokinetics of cetuximab delivered *via* the airways in wild-type (WT) and FcRn knockout (KO) mice, to evaluate the contribution of the neonatal Fc receptor (FcRn), which plays a key role in the distribution and recycling of IgG and the passage of mAbs from the lung into the bloodstream [23–29]. Finally, we evaluated the pharmacokinetic profile of aerosolized cetuximab in non-human primates, a relevant model for the aerosol delivery of cetuximab, for extrapolation of the results to humans.

2. Materials and methods

2.1. Orthotopic mouse model of lung cancer

Seven-week-old Balb/c nude mice were purchased from Janvier® (Saint-Berthevin, France) and used to establish an orthotopic model of bioluminescent lung tumors sensitive to cetuximab. The A549-Luc-c8 cell line was obtained from Perkin Elmer (Courtaboeuf, France). For tumor induction, the animals were anesthetized and placed on a frame with the head inclined upward at a 30° angle. A catheter (First PICC SL 1.9F 24 G × 50 cm, Apotecnia®, Aubagne, France) was inserted into the trachea *via* the mouth and 10^6 A549-Luc cells were injected into the lungs in 25 µl of serum-free medium containing 0.5 mM EDTA. Bioluminescence imaging (BLI) was performed 9 to 10 days later, with the IVIS-Lumina II imaging system (Perkin Elmer, Villebon sur Yvette, France), to check the quality of tumor induction and to allocate mice to homogeneous groups. All the studies using this model were approved by the ethics committee for animal experiments of the Val-de-Loire (no. 2012-04-10).

2.2. Antitumor efficacy

We administered 10 mg/kg cetuximab or 0.9% NaCl 10 days after the implantation of tumor cells, using a Microsprayer® IA-1b aerosolizer introduced orotracheally, as described above, once weekly for three weeks. Bioluminescence imaging was performed once weekly during treatment. At the end of the experiment, the animals were killed and their lungs were removed for histological analysis. Tumor volume was calculated as previously described [30].

2.3. Intratumor distribution of aerosolized cetuximab

Cetuximab (5 mg/mL) was conjugated to NHS-AF750 dye (cetuximab-IR dye) with an antibody labeling kit (SAIVI™ Rapid Antibody Labeling kits, Invitrogen, Cergy-Pontoise, France), according to the manufacturer's instructions. Fluorescent cetuximab (cetuximab-AF 750), at a dose of 10 mg/kg, was injected into the tail vein (50 µg mAb in 200 µl PBS) or directly into the lungs *via* the airways (50 µg in 50 µl PBS), in anesthetized A549-Luc tumor-bearing mice. After 2 h, 48 h and at various time points up to 42 days, the mice were anesthetized and fluorescence images were obtained from the live animal or from its lungs after it had been killed. Images were acquired with a Lumina II (Perkin Elmer) using dedicated filters (excitation: 745 ± 15 nm, emission: 800 ± 10 nm).

2.4. Fluorescence imaging

Given the major challenges involved in fluorescence quantification in the lungs, we used two different modes of fluorescence imaging. A new 3D fluorescence imager operating on true rotating tomography principles, the BioFLECT imager (Trifoil Imaging, Northridge, USA) was used, together with *ex vivo* measurements with the Lumina II (Perkin Elmer, Villebon sur Yvette, France). We first injected 500 IU heparin (Choay, Sanofi France) into the mice, to prevent coagulation when the mice were killed. Tomographic acquisitions were performed with the BioFLECT device. Mice were then imaged on the CT scanner of a NanoSPECT/CT scanner (Mediso, Budapest, Hungary) to obtain more details about anatomic locations. Accurate quantitative data were obtained by the 2D fluorescence imaging of lungs and dissected tumors and use of a calibration curve. For acquisition and reconstruction information, see the supplementary materials and methods.

2.5. Immunohistochemistry

For the detection of cetuximab-AF 750 in the cells of the lungs of A549-Luc tumor-bearing mice after 3D and 2D quantitative imaging, the fluorescent lungs were sampled, fixed by the intratracheal infusion of 10% neutral formalin for 1 h and the tumor was then excised, together with a similar volume of healthy tissue. The immunohistochemistry procedure is detailed in the supplementary materials. Briefly, cetuximab was detected on lung sections (8 µm) with the Vectastain Elite ABC kit for human IgG, as recommended by the manufacturer (Vector Laboratories, Nanterre, France).

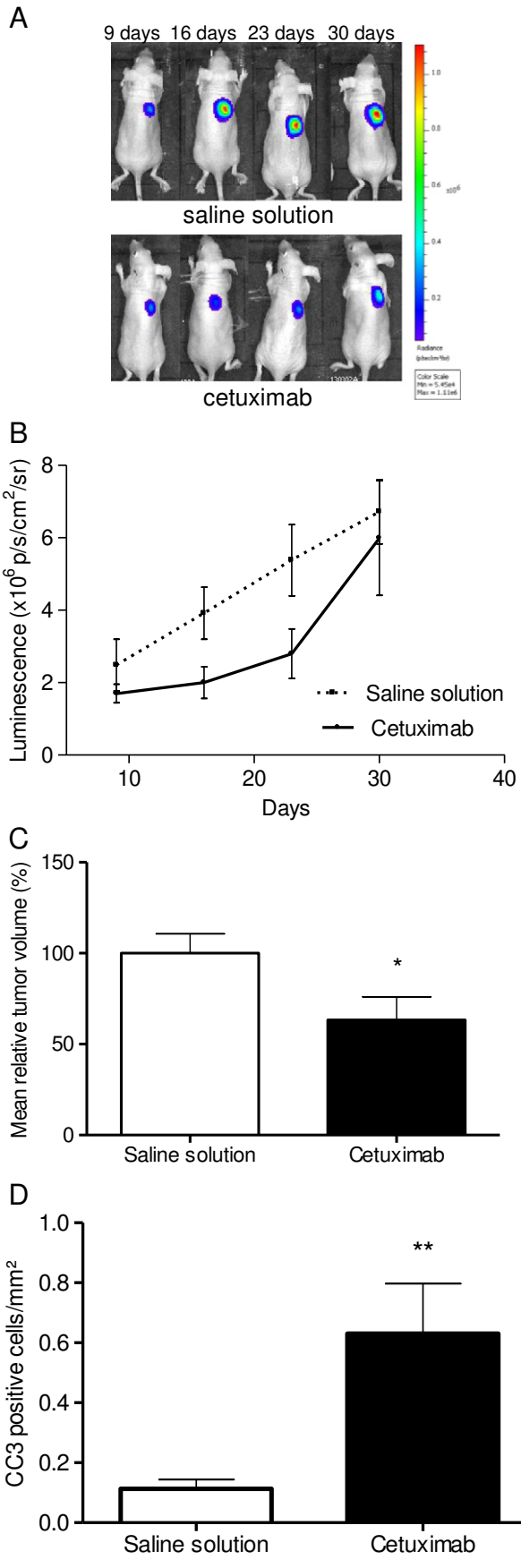

2.6. Administration of aerosolized cetuximab in WT and FcRn KO mice

Eight- to eleven-week-old (C56BL/6 WT and C56BL/6 FcRn KO) mice were obtained from Janvier® (Saint-Berthevin, France) and The Jackson Laboratory (Bar Harbor, Maine, USA), respectively. Cetuximab (5 mg/mL) was purchased from Merck KGaA (Darmstadt, Germany). All experiments were performed in accordance with national animal care guidelines (EC directive 86/609/CEE, French decree no. 87-848), and were approved by the ethics committee for animal experiments of the Val-de-Loire (no. 2012-04-9). We monitored body weight throughout the study, as an indicator of health status. WT mice and FcRn KO mice were anesthetized with 2.5% isoflurane. The mAbs were administered either as an aerosol, with a Microsprayer® Aerosolizer IA-1b (Penncentury, Philadelphia PA) introduced orotracheally, or systemically, by retro-orbital injection in anesthetized mice. Cetuximab was administered at a dose of 10 mg/kg, for both routes. Blood samples were collected by submandibular puncture at 2 h, 6 h, 1 day, 2 days, 3 days, 7 days, 15 days and 30 days. Blood samples were centrifuged at 1500 ×*g* for 15 min at 20 °C.

2.7. Administration of aerosolized cetuximab in non-human primates

Ten two-year-old female cynomolgus macaques, each weighing 3 kg, were obtained from Bioprim® (Baziege, France). This study was approved by the ethics committee for animal experiments of the Val-de-Loire (no. 2011-03-5).

Cetuximab was administered *via* the pulmonary or intravenous route, at a dose of 15 mg/kg, in macaques anesthetized by intramuscular injection of 0.5 mg/kg ketamine and 10 mg/kg xylazine. The animals receiving i.v. cetuximab also received an aerosol of saline solution. Cetuximab was aerosolized in six macaques, resulting in direct delivery to the tracheobronchial tree, with a Microsprayer® Model IA-1b Aerosolizer (PennCentury, Philadelphia, PA) inserted *via* a pediatric tracheal tube (Hi-contour™ with Brandt™ system; Tyco Healthcare, Gosport, United Kingdom). A total of 10 squirts of approximately 150 µl each were administered for the airway delivery of the mAb, as previously described [31]. Non-concentrated cetuximab was administered intravenously to two macaques, with an electric syringe pump, operating at a flow rate of 1 mL/min. Blood samples were collected at 2 h, 6 h, 24 h, 48 h, 72 h, 7 days, 15 days, 30 days and 45 days. Hematological and biochemical parameters were analyzed. At the end of the protocol, one monkey from each group was killed and the lungs, kidneys, liver and spleen were excised and analyzed for any signs of toxicity.

2.8. Pharmacokinetic analysis

Plasma concentrations of cetuximab were determined by ELISA, as previously described [32]. Pharmacokinetic analyses were performed by compartmental and non-compartmental approaches in mice. Compartmental pharmacokinetic analyses were performed by nonlinear mixed-effects modeling, with Monolix (version 4.2.2, Lixsoft) [33]. Non-compartmental pharmacokinetic analyses were performed with R software (version 3.0.1), with the "PK" package [34,35].

The compartmental approach describes the concentrations measured after administration *via* the two routes, for both FcRn WT and

Fig. 1. Anti-tumor response to cetuximab delivered *via* the pulmonary route in an orthotopic mouse model of human lung tumor. 1A. Bioluminescence images of A549-Luc tumor-bearing mice treated with a saline solution or cetuximab (0.25 mg/animal) administered *via* the pulmonary route. 1B. Kinetics of the mean light intensity of A549-Luc tumors in mice treated with a saline solution or cetuximab (0.25 mg/animal) administered *via* the pulmonary route. 1C. Mean of the relative volume of A549-Luc tumors on day 31, after the mice treated with a saline solution or cetuximab (0.25 mg/animal) *via* the pulmonary route had been killed. 1D. Immunohistochemical score for cleaved caspase-3 (CC3), corresponding to the number of positive cells per tumor surface, in the lung tumor area of mice treated with cetuximab or a saline solution *via* the airways. $^{*}p < 0.05$, $^{**}p < 0.001$.

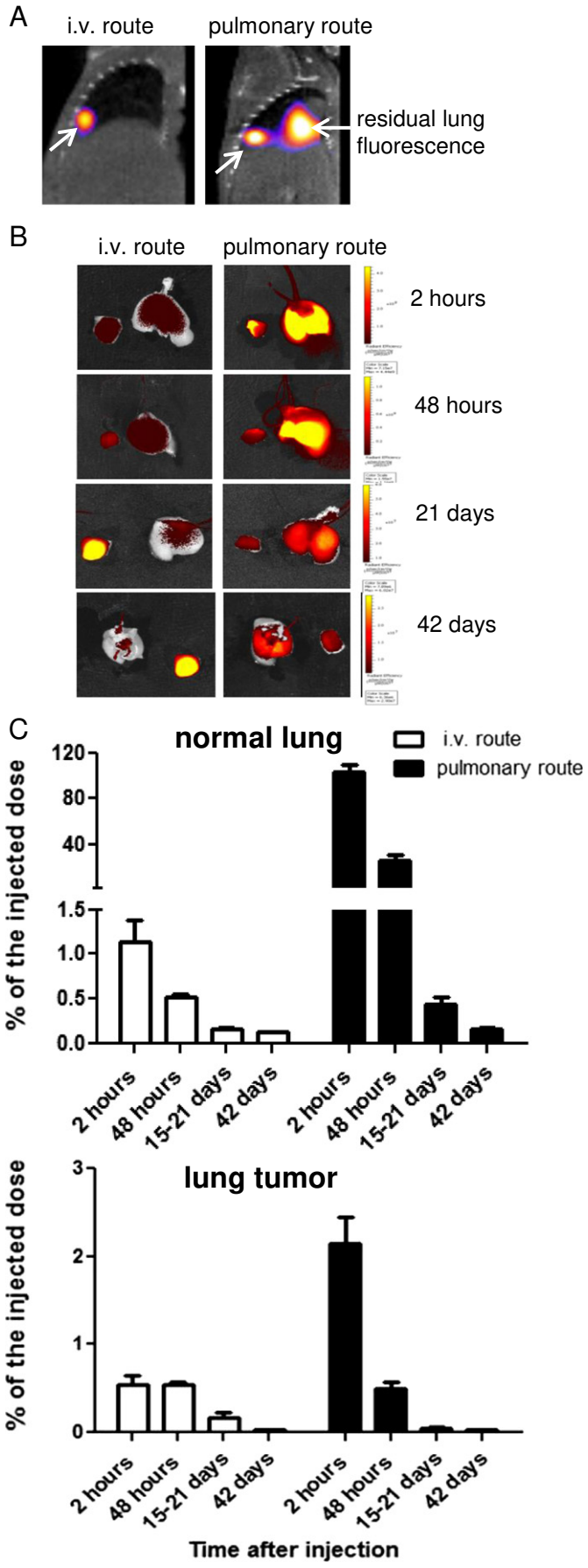

Table 1
Mean and SEM of the estimated proportion of the injected (as %) present in the lung and lung tumor, as determined by the quantification of fluorescence on excised specimens.

Time after injection	Normal lung		Lung tumor	
	I.v. route	Pulmonary route	I.v. route	Pulmonary route
2 h	1.13 ± 0.25	103.31 ± 6.27	0.54 ± 0.11	2.15 ± 0.29
48 h	0.52 ± 0.03	26.05 ± 4.05	0.55 ± 0.03	0.49 ± 0.09
15–21 days	0.16 ± 0.02	0.44 ± 0.08	0.18 ± 0.05	0.05 ± 0.01
42 days	0.13 ± 0.00	0.16 ± 0.02	0.03 ± 0.00	0.03 ± 0.00

KO mice, with the same model. This method optimizes the estimation of common parameters, and allows the quantification of FcRn-mediated distribution/elimination. Monoclonal antibodies were considered to be distributed between three compartments: 'L' (lung) is the compartment of administration for the orotracheal route; 'C' (central) is the compartment of administration for the i.v. route, for which plasma mAb concentrations were determined; and 'P' is the peripheral compartment. Redistribution from compartment x to compartment y is characterized by a first-order transfer rate constant, k_{xy} (Fig. 4C). A lung bioavailable fraction F_L was also estimated. The differences in mAb pharmacokinetics between WT and FcRn KO mice were taken into account by allowing the fraction not bound to FcRn (fu) to vary between 0 and 1. If the value of fu is low, k_{outC} and k_{outP} mostly result in a transfer (recycling) of mAbs from compartments 'C' to "L" and and 'P' to "C", respectively. If the value of fu is high, k_{outC} and k_{outP} mostly lead to the elimination of mAbs. The non-compartmental approach described the pharmacokinetic profiles in terms of the area under the concentration–time curve (AUC in $mg \cdot L^{-1} \cdot day$), the area under the first moment of the concentration-time curve ($AUMC$ in $mg \cdot L^{-1} \cdot day^2$), mean residence time ($MRT$ in days), half-life for elimination ($t_{1/2}$ in days), mean absorption time (MAT in days) and the bioavailable fraction (F in %).

2.9. Statistical analysis

Continuous values are expressed as means ± SEM. Two-tailed Mann–Whitney tests were performed for comparisons of bioluminescence, tumor volume and numbers of cleaved caspase-3-positive cells between the aerosolized cetuximab and placebo groups, in mice. This test was also used to compare subcutaneous tumor volumes between the pulmonary cetuximab and placebo groups in mice. We considered p values ≤ 0.05 to be statistically significant.

3. Results

3.1. Mouse model of a bioluminescent lung tumor sensitive to cetuximab

Cetuximab binds with high affinity to the epidermal growth factor receptors (EGFRs) of both humans and macaques, but not to the rodent ortholog [36,37]. We analyzed the amount of cetuximab deposited on its target antigen site and the cellular distribution of this mAb within the lungs after direct delivery to the lungs, by developing a mouse model of lung tumor. A549-Luc cells – human alveolar adenocarcinoma

Fig. 2. Lung distribution of cetuximab-AF 750 delivered by the i.v. or pulmonary route in A549-Luc tumor-bearing mice. 2A. Representative bimodal images of the lungs (sagittal views) combining fluorescence tomography and CT scans for animals receiving a single i.v. (13 days) or pulmonary (48 h) administration of cetuximab-AF 750. Arrows indicate the position of the lung tumor. 2B. *Ex vivo* fluorescence images of the lungs of A549-Luc tumor-bearing mice, after tracer injection (cetuximab-AF 750). One representative specimen is presented for each imaging time. The color scales are not the same for all charts because of the decrease in fluorescence intensity over time. However, all images are comparable for a given chart. 2C. Estimated proportion of the injected dose of cetuximab-AF 750 (%) in the normal lung tissue and the tumor, after a single administration *via* the i.v. and pulmonary routes. For each time point, $n = 3$ to 6, except for 42 days, when $n = 1$ and 2 for the i.v. and pulmonary routes, respectively. At 24 h, a profile similar to the one of 48 h was observed (data not shown). Results are expressed as means and SEM.

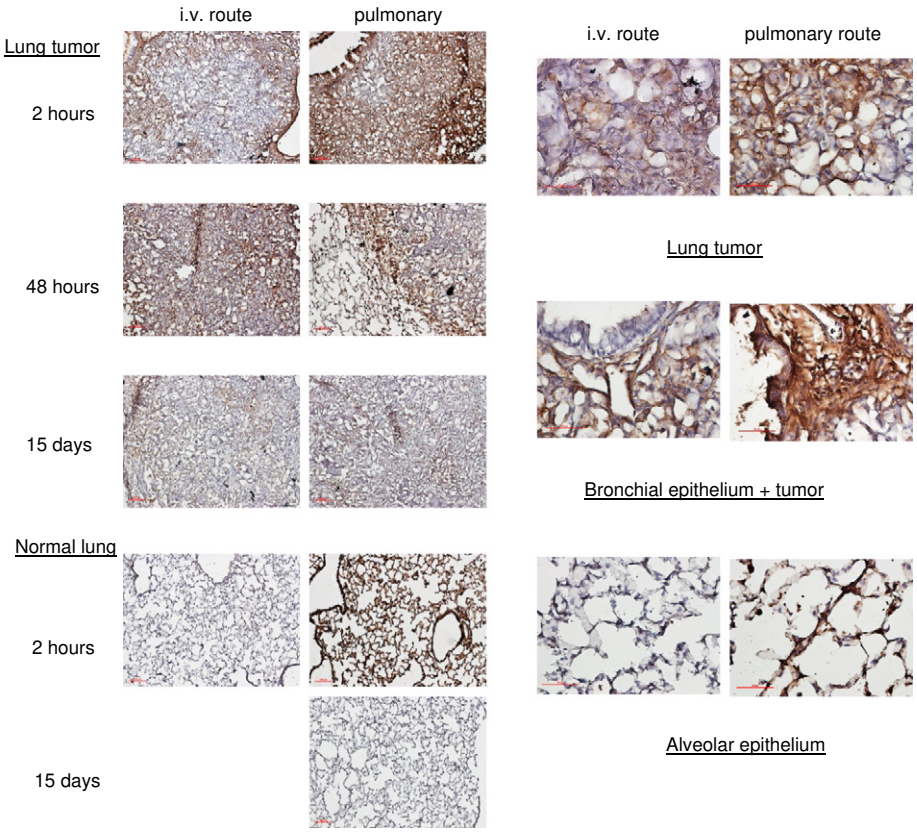

Fig. 3. Immunohistochemistry analysis of cetuximab-AF 750 in the normal lung tissue and in the lung tumor after a single administration *via* the i.v. and pulmonary routes. Kinetics of cetuximab distribution in normal airways and the tumor after i.v. or pulmonary delivery (left panel) (magnification ×10, red scale = 100 μm). High-magnification (×40, red scale = 50 μm) images of cetuximab deposition in the lungs after i.v. or pulmonary delivery, obtained at 48 h (right panel).

cells transfected with luciferase – were used for the establishment of this model, because they display significant levels of EGFR expression at their surface and are sensitive to cetuximab *in vitro* (Supplementary data). Moreover, the implantation and growth of A549-Luc tumors can be followed by monitoring bioluminescence. Ten days after tumor induction, mice were separated into two homogeneous groups and treated with aerosols of either cetuximab or a saline solution once weekly for three weeks. Tumor growth was monitored by weekly bioluminescence imaging and by the post mortem measurement of tumor volume (Fig. 1A).

Mean tumor bioluminescence before treatment was similar in the two groups. On days 16 and 23, the mean bioluminescence signal was significantly weaker for the group treated with aerosolized cetuximab than for the group treated with placebo (Fig. 1B). On day 16, the mean ± SEM bioluminescence was $2.003 \times 10^6 \pm 0.436 \times 10^6$ and $3.917 \pm 0.718 \times 10^6$ p/s/cm^2/sr for aerosolized cetuximab and placebo, respectively ($p \leq 0.05$) (Fig. 1B). On day 23, mean ± SEM bioluminescence was $2.798 \times 10^6 \pm 0.683 \times 10^6$ and $5.640 \times 10^6 \pm 0.927 \times 10^6$ p/s/cm^2/sr for aerosolized cetuximab and placebo, respectively ($p \leq 0.05$). On day 30, mean bioluminescence was lower in the aerosolized cetuximab group, but this difference was not statistically significant. The intensity of bioluminescence might not reflect tumor growth when the tumor becomes hypoxic or necrotic [38]. We therefore also evaluated tumor volume by histopathological analysis. Mean tumor volume was significantly lower in the cetuximab-treated animals than in the control animals (Fig. 1C). The difference in tumor volume between the two groups of animals was 37% at the end of the study ($p \leq 0.05$). We explored the molecular mechanisms of apoptosis associated with tumor reduction, by evaluating cetuximab-induced apoptosis by the immunohistochemical investigation of caspase-3 cleavage in the lungs of animals treated with aerosolized saline buffer or cetuximab. In the tumor area, the mean number of cleaved caspase-positive cells/mm^2 was 0.113 ± 0.030 in the cetuximab-treated mice and 0.630 ± 0.167 in the placebo-treated mice ($p < 0.001$) (Fig. 1D). The higher levels of cleaved caspase-3 in the cetuximab group are consistent with the tumor reduction observed in this group. These results demonstrate that this model is robust enough for evaluation of the distribution of cetuximab in the target tumor tissue.

3.2. Distribution of mAb to its target antigen after delivery via the airways

Much less is known about the biodistribution of mAbs after airway delivery than after i.v. injection. We analyzed the distribution of cetuximab in the A549-Luc lung tumor model, which is sensitive to cetuximab. Cetuximab was conjugated to an infrared dye (cetuximab-750-IRdye) and administered by the i.v. or pulmonary route, in A549-Luc tumor-bearing mice. The distribution of the antibody was analyzed by near-infrared imaging (NIRF). The 2D and 3D fluorescence images showed the effective deposition of cetuximab-IR dye in the tumor for both routes (Fig. 2A and B).

At 2 h, the amount of cetuximab in the lung tumor, as determined by fluorescence imaging, was 2.15 ± 0.29% and 0.54 ± 0.11% of the dose administered for the pulmonary and i.v. routes, respectively (Table 1). After this time point, the distribution of cetuximab was similar for both routes of administration (Fig. 2C and Table 1), as expected, given that A549-Luc cells are the only specific target of cetuximab, limiting the non-pulmonary binding of the mAbs delivered i.v. In normal lungs, an early, marked and durable accumulation of cetuximab was observed after pulmonary delivery but not after i.v. injection (Fig. 2C and Table 1).

Immunohistochemical analyses showed that the spatial distribution of cetuximab within the tumor was similar for the two routes of administration (Fig. 3). The only difference was the accumulation of

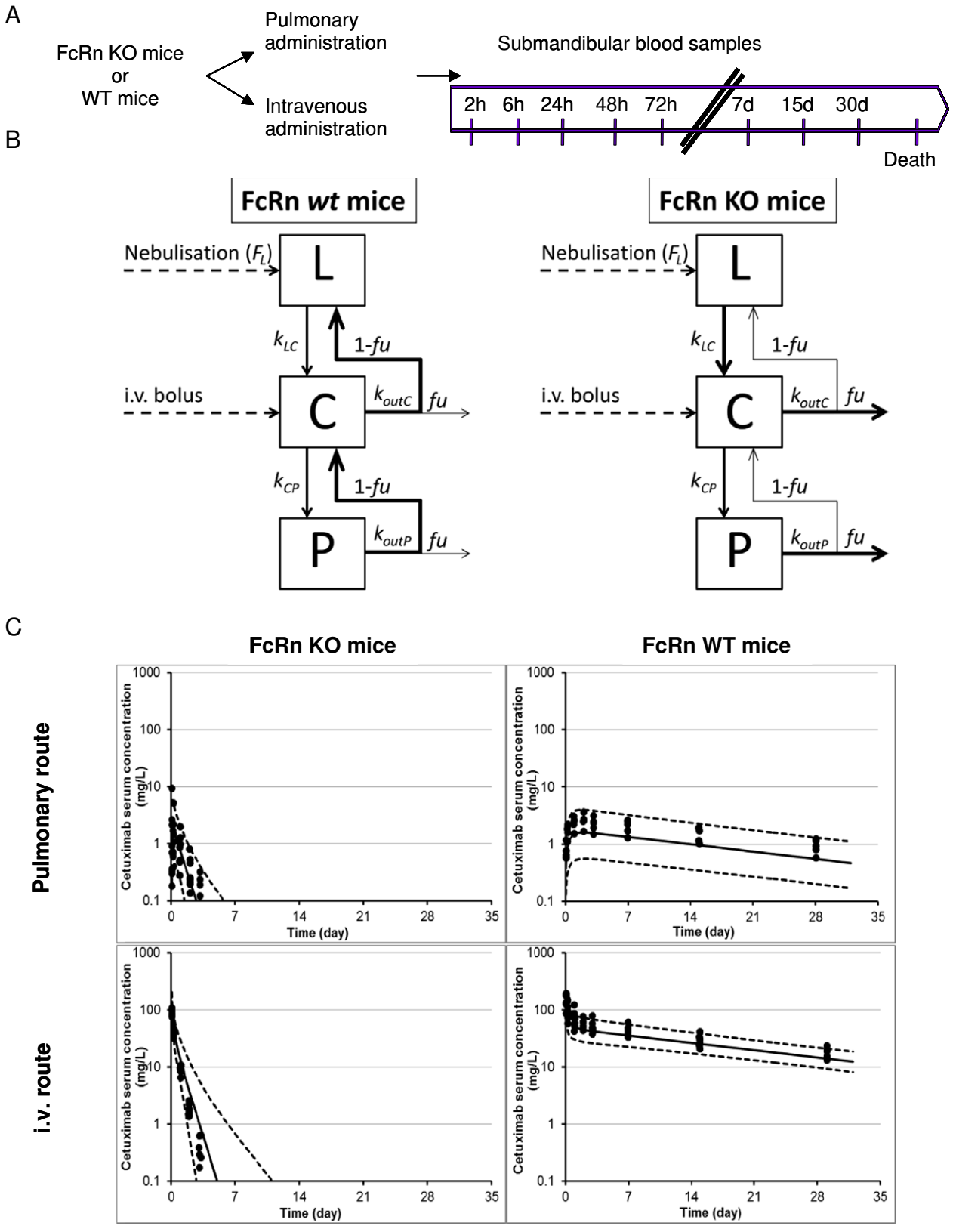

Fig. 4. Pharmacokinetics of cetuximab delivered *via* the airways in WT and FcRn KO mice. 4A. Schematic representation of the protocol. 4B. Schematic representation of the mechanistic model used to describe cetuximab pharmacokinetics after pulmonary or systemic administration in FcRn WT (left) and FcRn KO (right) mice. mAbs are distributed between three virtual compartments: – 'L' is the compartment of administration *via* the pulmonary route. – 'C' is the compartment of administration for the i.v. route and the compartment in which mAb concentrations were determined. – 'P' is the peripheral compartment. Redistribution from compartment *x* to compartment *y* is characterized by a transfer rate constant k_{xy}. The high value of the *fu* parameter for FcRn KO mice leads to faster elimination of the mAb. 4C. Visual predictive checking of the cetuximab time–concentration profiles following single injection (i.v. or pulmonary) in mice. Dots correspond to observed cetuximab concentrations. The solid curves and the gray area are the median and the 90% intervals for all simulated groups, respectively.

Table 2
Estimated non-compartmental pharmacokinetic parameters for cetuximab in WT and FcRn KO mice. AUC: area under the concentration–time curve; AUMC: area under the first-moment concentration–time curve; MRT: mean residence time; $t_{1/2}$: half-life for elimination; MAT: mean absorption time; F: bioavailable fraction.

	CETUXIMAB	
	FcRn WT	FcRn KO
I.v. route	n = 8	n = 7
$AUC_{0\rightarrow\infty}$ ($mg \cdot L^{-1} \cdot day$)	942.9	39.0
$AUMC_{0\rightarrow\infty}$ ($mg \cdot L^{-1} \cdot day^2$)	9851.4	19.4
MRT (day)	10.4	0.5
$t_{½}$ (day)	7.2	0.3
Pulmonary route	n = 9	n = 9
$AUC_{0\rightarrow\infty}$ ($mg \cdot L^{-1} \cdot day$)	37.0	3.1
$AUMC_{0\rightarrow\infty}$ ($mg \cdot L^{-1} \cdot day^2$)	456.8	3.8
MRT (day)	12.4	1.2
$t_{½}$ (day)	8.6	0.9
F	3.9%	7.9%
MAT (day)	1.9	0.7

cetuximab in the bronchial and alveolar region after airway delivery, with no detection of cetuximab in the normal lung after i.v. injection (Fig. 3). Cetuximab was detected in the lumen surrounding bronchial epithelial cells and in immune cells in the normal mouse lung.

3.3. PK of mAbs delivered via the airways: impact of FcRn expression

The passage of mAbs from the lungs into the bloodstream probably results from FcRn-mediated capillary absorption, as previously reported for proteins conjugated to the Fc domain of IgG [26,39]. We evaluated the contribution of FcRn to the bioavailability of mAbs after airway delivery, by analyzing the PK parameters of cetuximab delivered to WT and FcRn KO mice by a non-compartmental approach (Fig. 4A), using i.v. injection as the control route. Overall, the animals tolerated well cetuximab delivery and the experimental procedure.

3.4. Intravenous route

Plasma cetuximab concentrations peaked 2 h after systemic delivery in both WT and FcRn KO mice (Fig. 4 and Supplementary Fig. 3). Elimination profiles differed between WT and FcRn KO animals. As expected, cetuximab was no longer detectable seven days after administration in FcRn KO mice, whereas it was detected in the blood of WT mice until day 30, the last time point in the study. A non-compartmental pharmacokinetic analysis was performed and the estimated mean residence time (MRT) was greater in WT mice than in FcRn KO mice: 10.4 and 0.5 days, respectively (Table 2). The half-life of the mAb was 7.2 days in WT mice and 0.3 days in FcRn KO mice.

Table 3
Estimated compartmental PK population parameters (Fig. 4B) for cetuximab in WT and FcRn KO mice. CV% is the interindividual variability. r.s.e. (%) is the relative standard error in percentage. a and b are the additive and proportional parameters of the residual error model, respectively.

Parameter	Value (CV%)	r.s.e. (%)
F_L (%)	3.53 (23)	16
$k_{LC(FcRn\,=\,wt)}$ (day^{-1})	1 (94)	7
$k_{LC(FcRn\,=\,KO)}$ (day^{-1})	3.4 (23)	26
V_1 (mL)	1.1 (24)	5
k_{CP} (day^{-1})	6.64 (−)	1
k_{outC} (day^{-1})	2.08 (−)	1
k_{outP} (day^{-1})	5.08 (51)	12
$fu_{FcRn\,=\,wt}$ (%)	2.18 (1)	2
$fu_{FcRn\,=\,KO}$ (%)	43.9 (26)	8
a	0.007	35
b	0.115	8

3.5. Pulmonary route

After pulmonary delivery, plasma cetuximab concentration peaked very early, after 2 h, in FcRn KO mice, and later, at one day, in WT mice (Fig. 4 and Supplementary Fig. 3). Surprisingly, the non-compartmental pharmacokinetic analysis showed that the bioavailability of cetuximab was lower in WT mice than in FcRn KO mice: 7.9% and 3.9% in FcRn KO and WT mice, respectively (Table 2). The elimination profiles also differed radically between WT and FcRn KO mice. Cetuximab was not detectable at 7 days in FcRn KO mice, whereas it remained detectable until day 30 in WT mice. The MRT was longer in WT mice than in FcRn KO mice (10.4 and 0.3 days, respectively). Moreover, the mean absorption time was very short in FcRn KO mice, at an estimated 0.7 days, and was much shorter than the 1.9 days recorded for WT mice. Similar results were obtained with rituximab, another chimeric mAb without a target antigen in mice (Supplementary Fig. 3, and Supplementary Table 1).

A semi-mechanistic PK model was developed, to describe the serum concentration-time profiles of the mAb in WT and FcRn KO mice (Fig. 4B). The transfer of mAbs between the lung and central compartments was mostly in the direction of the lung for WT mice and in the direction of the central compartment for KO mice (Table 3). The estimated PK parameters indicated that the larger fraction of mAb not bound to FcRn (fu) in FcRn KO mice as compared to WT mice led to the faster elimination of the mAb (Fig. 4C and Table 3). Elimination rates for cetuximab (fu_{KO}/fu_{WT}) were thus 20 times higher in FcRn KO mice than in FcRn WT mice. Similar results were obtained for rituximab delivered i.v. and *via* the airways (Supplementary Table 2).

3.6. Comparison of pharmacokinetics in mice and non-human primates

Non-human primates are often used for PK analyses of mAbs and in aerosol studies because of their immunological and anatomical similarities to humans. We analyzed the PK parameters of cetuximab in 8 macaques, each of which received a single administration of cetuximab *via* the i.v. ($n = 2$) or the pulmonary ($n = 6$) route. The procedure is detailed in Fig. 5A. Single doses of cetuximab delivered *via* the airways were well tolerated, as shown by the absence of significant variation for the weight, biochemical and hematological parameters (Fig. 5B). Moreover, the pathologists saw no sign of toxicity or of lesions in the lungs excised from two animals killed after the administration of cetuximab *via* the airways.

The dose of 15 mg/kg used here lies in the range for which the dose–response relationship is nonlinear. Cetuximab displayed a biphasic bioavailability profile after i.v. injection, with a rapid distribution phase followed by a prolonged elimination phase (Fig. 6). After airway delivery, cetuximab was absorbed slowly and in only small amounts, with even lower levels found in the bloodstream than in mice. The compartmental approach was not possible, because of the high heterogeneity of PK profiles and the small number of animals. With the exception of one macaque that inhaled gastric liquid during aerosol delivery and displayed a high level of mAb passage into the bloodstream (Supplementary Fig. 4), PK analyses by a non-compartmental approach indicated that the bioavailability of cetuximab in serum after pulmonary administration (F) was low, even lower than that in rodents, at only 0.3% (Table 4). The mean residence time (MRT) in serum was 2.8 days and the mean absorption time (MAT) was 8.1 days, these values being different from those for rodents.

4. Discussion

The route of administration may be critical to optimize the benefits of mAbs in respiratory diseases. We evaluated the processes occurring after the deposition of the aerosolized mAbs in the lungs. Our findings clearly demonstrate that the airways are a relevant route of administration for improving the therapeutic index of mAbs, increasing their

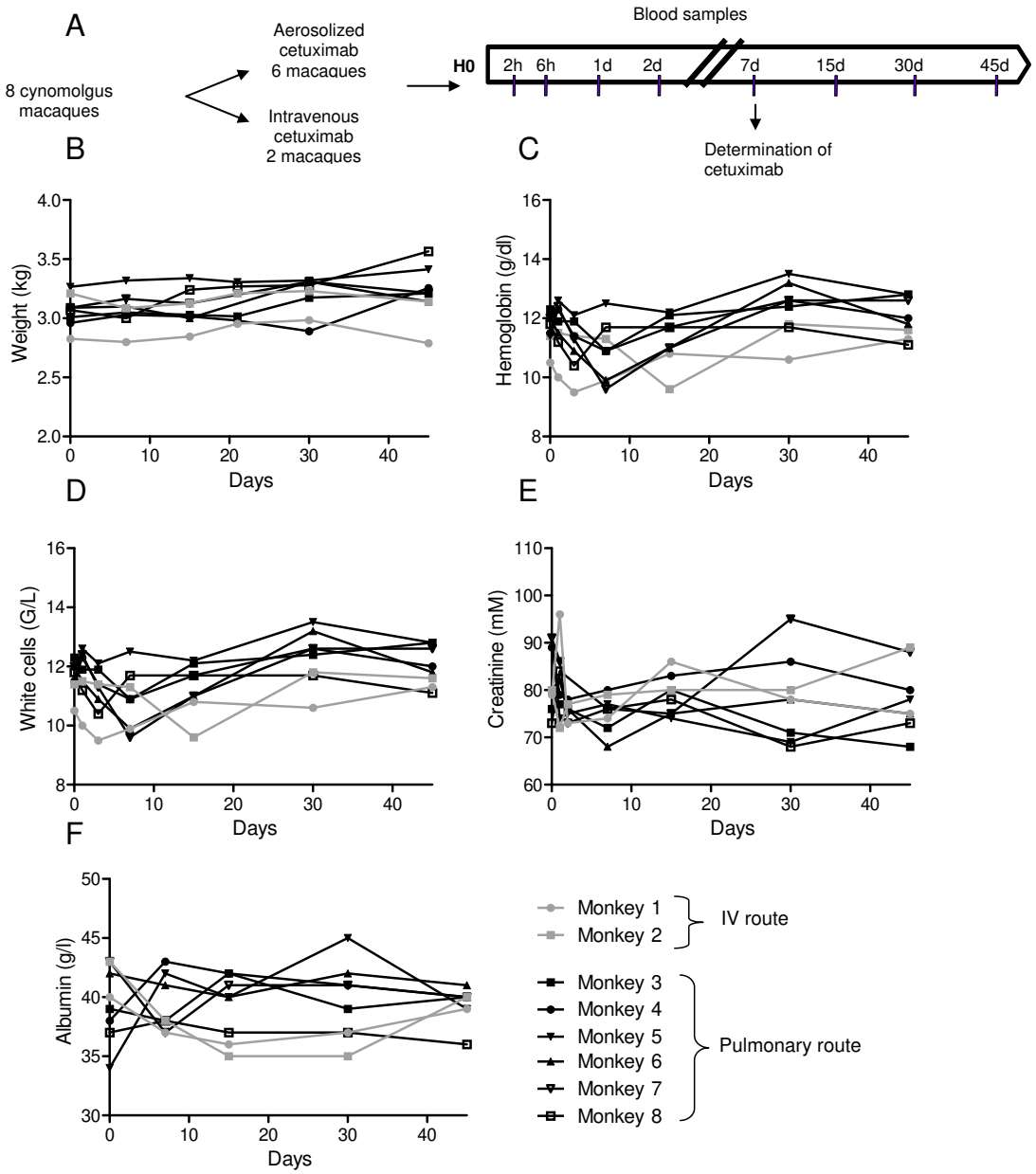

Fig. 5. Tolerance profile of aerosolized cetuximab in non-human primates. 5A. Schematic representation of the protocol. 5B–F. Weight, hematological and biochemical parameters measured in macaques after the intravenous or airway delivery of cetuximab.

concentration within the target organ while limiting their passage into the bloodstream.

We first developed a murine model of a bioluminescent human lung tumor sensitive to cetuximab. In this model, the once weekly intrapulmonary administration of cetuximab significantly limited lung tumor progression. Consistent with previous results showing that the cetuximab-induced antitumor response is due partly to apoptosis, we found a marked increase in the levels of cleaved caspase-3, a central mediator and marker of apoptosis, in the tumor cells of mice treated with aerosol-delivered cetuximab [40–42]. This suggests that the molecular mechanisms of cetuximab action are independent of the route of administration. This model, in which we were able to demonstrate an objective therapeutic response to airway-delivered cetuximab was then used to quantify cetuximab distribution in the lungs and the tumor after pulmonary delivery.

We used a combination of quantitative and qualitative methods to assess the distribution of cetuximab. Whole-body fluorescence tomography with a near-infrared fluorochrome was carried out with a next-generation 3D imaging device, to determine the location of cetuximab in the lung and the tumor. This method is particularly suitable for the imaging of mAbs with low clearance rates in blood and for which radioisotopic imaging methods, such as PET and SPECT, are not appropriate for long-terms studies, such as studies of biodistribution, pharmacokinetics and the determination of residence time at the tumor target. Near-infrared fluorescence imaging is highly suitable for the *in vivo* imaging of deposition or targeting in the lung. However, accurate quantification remains difficult, due to the characteristics of this organ, particularly as concerns the absorption and diffusion of photons. We therefore used a combination of 3D *in vivo* imaging and 2D quantification on *ex-vivo* lung specimens to determine the amount of cetuximab in the target tissue. We also used immunohistochemical analysis to determine the location of cetuximab in the lung and target tumor tissue more precisely. We found that cetuximab reached the tumor, and that tumor uptake was time-dependent after both systemic and pulmonary administrations. However, the profiles of cetuximab uptake into the tumor and the normal lung depended on the route of administration.

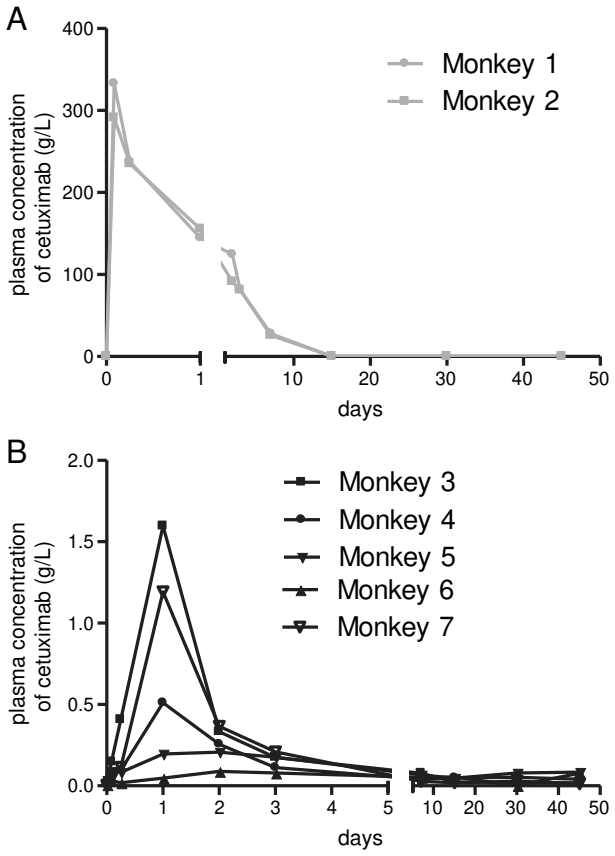

Fig. 6. Plasma concentration and pharmacokinetic model of cetuximab delivered *via* the pulmonary and i.v. routes in non-human primates. 6A. Mean plasma concentration over time following single i.v. administrations of cetuximab in macaques. 6B. Mean plasma concentration over time following single airway administrations of cetuximab in macaques.

The mAb accumulated rapidly in these tissues after airway delivery, at concentrations twice those for the i.v. route at early time points. Cetuximab reached the target tumor tissue more slowly after i.v. injection. These results suggest that aerosol delivery is potentially relevant for administration of anticancer mAbs with a dose-dependent mechanism of action. After 48 h, the concentration of cetuximab in the tumor was similar for the two routes, as expected given the model used. Indeed, cetuximab can bind only to A549-Luc in this animal model and it therefore concentrated in the tumor after i.v. injection. The tumor lesions in this model were small, but the spatial distribution of cetuximab within the tumor was nevertheless heterogeneous, as previously reported for other mAbs [43–46].

After i.v. injection, mAb penetration is often limited to perivascular spaces, and several parameters, such as mAb affinity, antigen expression and internalization and hypoxia, have been shown to influence their distribution within solid tumors [43–45]. After pulmonary delivery, cetuximab staining was more pronounced at the edges of the respiratory branches, undoubtedly due to the large amounts of mAb accumulating in the airways. Given these differences in spatial distribution, it might be interesting to combine the two delivery routes (i.v. and pulmonary) to improve mAb distribution within lung tumors. The pulmonary route, whether used alone or in combination with standard i.v. treatments, would be particularly useful for the treatment of lepidic lung adenocarcinomas, which are generally excluded from clinical trials.

Small drugs delivered *via* the pulmonary route have been shown to have short retention times in the lungs, due to massive and rapid passage into the systemic circulation through passive diffusion [47–49]. By contrast, we previously demonstrated that cetuximab entered the bloodstream only very slowly and in small amounts after aerosol delivery [17]. Other groups showed that the bioavailability of Fc-fusion proteins (erythropoietin, FSH, IFNβ, IFNα) may depend on the size and structure of the molecules [27,28]. With erythropoietin, they have reported a similar limited bioavailability of dimeric Fc fusion molecule (5–10% in primates and human) as opposed to the high transfer into the bloodstream of the monomer configuration (around 30%) [39]. The mechanisms involved in the passage of mAbs from the lungs into the bloodstream are not fully understood. FcRn, a receptor that binds IgG, plays a key role in the pharmacokinetics of mAbs, contributing to their recycling and transcytosis [23–25]. In the lungs, the expression of this receptor is restricted to the epithelial cells of the upper airways and alveolar macrophages in humans and macaques, whereas it is also detected in the epithelium of the alveolar region in rodents [21,24]. Previous studies with Fc-fusion proteins clearly incriminated FcRn in this transepithelial transport mutating amino acids in the Fc domain critical for FcRn binding [39]. In this study, we used WT and FcRn KO mice to investigate the precise contribution of FcRn to the transfer of mAbs delivered *via* the airways from the lungs to the bloodstream. The bioavailability of mAbs was low after pulmonary delivery in WT animals but, surprisingly, it was twice as high in FcRn KO animals. This indicates that FcRn is not the only factor involved in the transfer of mAbs to the bloodstream. Lymph drainage, which is involved in the uptake of large molecules, probably also contributes to the absorption of mAbs from the lungs, potentially accounting for the rapid passage of mAbs into the bloodstream after pulmonary delivery in FcRn KO mice. This hypothesis is supported by the detection of exogenous mAbs in lymph vessels after regional intestinal delivery [50]. The pharmacokinetic model also highlighted a 10 times longer mean residence time of mAbs in the lungs of WT mice than in those of FcRn KO animals. Overall, our results suggest that FcRn may make a greater contribution to mAb recycling than to IgG transcytosis in the airways. Furthermore, they suggest that

Table 4
Non compartmental pharmacokinetic analysis of cetuximab administered *via* the i.v. or pulmonary route in macaques. AUC: area under the concentration–time curve; AUMC: area under the first-moment concentration–time curve; MRT: mean residence time; $t_{1/2}$: half-life for elimination; MAT: mean absorption time; F: bioavailable fraction.

	AUC ($mg \cdot L^{-1} \cdot day$)	AUMC ($mg \cdot L^{-1} \cdot day^2$)	MRT (day)	Mean AUC ($mg \cdot L^{-1} \cdot day$)	Mean AUMC ($mg \cdot L^{-1} \cdot day^2$)	Mean MRT (day)	Mean MAT (day)	Mean $t_{1/2}\beta$ (day)	F (%)
I.v. route									
Monkey 1	771.73	2201.93	2.9	751.4	2130.3	2.8	–	1.96	0.3%
Monkey 2	731.01	2058.67	2.8						
Pulmonary route									
Monkey 3	2.84	23.41	8.2	2.1	21.8	10.9	8.1		
Monkey 4	2.42	6.95	2.9						
Monkey 5	1.32	13.30	10.1						
Monkey 6	1.87	28.38	15.1						
Monkey 7	2.02	36.93	18.3						

FcRn may mediate the excretion into the lumen of mAbs from lung tissue.

Additional experiments were performed in macaques, a relevant animal species anatomically and immunologically closer to humans, to facilitate the extrapolation of PK results to humans. In macaques, a single dose of cetuximab delivered *via* the airways was well tolerated and had a low bioavailability (0.3% of the dose administered), consistent with findings for dimeric Fc-conjugated proteins [27]. Moreover, aerosolized cetuximab was eliminated more rapidly in macaques than in mice (1.96 *vs.* 8.9 days), consistent with the binding of cetuximab to the simian EGFR, which is strongly expressed in the bronchi and probably contributes to mAb elimination, through effects on target-mediated drug disposition [51]. The antigen-dependent elimination of cetuximab and the restriction of FcRn expression to the upper airways in macaques may account for the difference in bioavailability between rodents and macaques, and for the inter-individual variability of absorption in macaques.

Numerous mAbs for respiratory diseases, such as asthma and idiopathic pulmonary fibrosis, are being developed and some are already at the clinical trial stage [52,53]. The standard delivery route for all these mAbs is i.v. injection. However, less invasive routes of administration are being investigated for the treatment of long-term chronic diseases [54]. Airway delivery is often used for the ambulatory treatment of patients with respiratory diseases and could therefore be considered for the local delivery of mAbs [55,56]. Overall, our results demonstrate that the administration of mAbs *via* the airways is effective, and well tolerated, leading to sustained high levels of accumulation in the lungs and only very slow absorption of small amounts of the mAb into the bloodstream. The pulmonary route may therefore constitute an attractive alternative to the systemic delivery of full-length mAbs for the treatment of outpatients with chronic respiratory diseases. This conclusion is supported by the findings of several preclinical studies of inhaled recombinant interleukin-derived products and anti-IL-13 Fab′ fragments, which have given promising results in human trials and animal models of asthma [20]. The pulmonary route may also be valuable for boosting the concentration of mAbs in the lungs over short periods of time. This may be crucial in infectious diseases of the respiratory tract, to inactivate the pathogen rapidly and prevent host tissue damage. Collectively, these data suggest that additional studies, including clinical trials in particular, should be carried out, to provide guidance on the therapeutic indications for the airway delivery of mAbs.

5. Conclusion

Biotherapies constitute the fastest growing sector of approved drugs. As a result, there is increasing interest in their regional delivery to the lungs *via* the airways, to increase therapeutic benefits to patients and to facilitate self-administration, which is both convenient and cost-effective. Our findings add new pieces to the "proof-of-concept" puzzle, demonstrating the efficacy of this route of delivery and providing information about the fate of inhaled mAbs in the treatment of respiratory diseases. They will undoubtedly contribute to the future development of inhaled mAbs for the treatment of respiratory diseases, for which there is still a significant unmet medical need.

Acknowledgments

We thank the PST Animaleries (Université de Tours, France) for technical assistance and advice with animal experiments. We also thank Flora Paul for her technical and kind assistance for immunohistochemistry. This work was supported by various sources of funding. N.HV received financial support from the French Higher Education and Research Ministry under the program "Investissements d'avenir", Grant agreement: LabEX MAbImprove ANR-10-LABX-53-01, from ARAIR (Tours, France), from Région Centre (Grant AeroMac and StabioMed) and the European Union (Grant Agreement: Presage 4940-37478; OutExFon). Europe is engaged in Région Centre with the FEDER. L.G. was supported by Le Fonds de Dotation "Recherche en Santé Respiratoire".

References

[1] P.E. Lipsky, D.M. van der Heijde, E.W. St Clair, D.E. Furst, F.C. Breedveld, J.R. Kalden, et al., Infliximab and methotrexate in the treatment of rheumatoid arthritis. Anti-Tumor Necrosis Factor Trial in Rheumatoid Arthritis with Concomitant Therapy Study Group, N. Engl. J. Med. 343 (2000) 1594–1602. http://dx.doi.org/10.1056/NEJM200011303432202.

[2] A.M. Scott, J.D. Wolchok, L.J. Old, Antibody therapy of cancer, Nat. Rev. Cancer 12 (2012) 278–287. http://dx.doi.org/10.1038/nrc3236.

[3] J.F. Colombel, W.J. Sandborn, W. Reinisch, G.J. Mantzaris, A. Kornbluth, D. Rachmilewitz, et al., Infliximab, azathioprine, or combination therapy for Crohn's disease, N. Engl. J. Med. 362 (2010) 1383–1395. http://dx.doi.org/10.1056/NEJMoa0904492.

[4] J.M. Reichert, Antibodies to watch in 2014, MAbs 6 (2014) 5–14. http://dx.doi.org/10.4161/mabs.27333.

[5] A. Jemal, R. Siegel, E. Ward, Y. Hao, J. Xu, T. Murray, et al., Cancer statistics, 2008, CA Cancer J. Clin. 58 (2008) 71–96. http://dx.doi.org/10.3322/CA.2007.0010.

[6] A.D. Lopez, K. Shibuya, C. Rao, C.D. Mathers, A.L. Hansell, L.S. Held, et al., Chronic obstructive pulmonary disease: current burden and future projections, Eur. Respir. J. 27 (2006) 397–412. http://dx.doi.org/10.1183/09031936.06.00025805.

[7] B. Ley, H.R. Collard, T.E. King, Clinical course and prediction of survival in idiopathic pulmonary fibrosis, Am. J. Respir. Crit. Care Med. 183 (2011) 431–440. http://dx.doi.org/10.1164/rccm.201006-0894CI.

[8] T. Koleba, M.H.H. Ensom, Pharmacokinetics of intravenous immunoglobulin: a systematic review, Pharmacotherapy 26 (2006) 813–827. http://dx.doi.org/10.1592/phco.26.6.813.

[9] T.K. Hart, R.M. Cook, P. Zia-Amirhosseini, E. Minthorn, T.S. Sellers, B.E. Maleeff, et al., Preclinical efficacy and safety of mepolizumab (SB-240563), a humanized monoclonal antibody to IL-5, in cynomolgus monkeys, J. Allergy Clin. Immunol. 108 (2001) 250–257. http://dx.doi.org/10.1067/mai.2001.116576.

[10] T.T. Hansel, H. Kropshofer, T. Singer, J.A. Mitchell, A.J.T. George, The safety and side effects of monoclonal antibodies, Nat. Rev. Drug Discov. 9 (2010) 325–338. http://dx.doi.org/10.1038/nrd3003.

[11] J. Boe, J.H. Dennis, B.R. O'Driscoll, T.T. Bauer, M. Carone, B. Dautzenberg, et al., European Respiratory Society Guidelines on the use of nebulizers, Eur. Respir. J. 18 (2001) 228–242.

[12] J. Vestbo, S.S. Hurd, A.G. Agustí, P.W. Jones, C. Vogelmeier, A. Anzueto, et al., Global strategy for the diagnosis, management, and prevention of chronic obstructive pulmonary disease: GOLD executive summary, Am. J. Respir. Crit. Care Med. 187 (2013) 347–365. http://dx.doi.org/10.1164/rccm.201204-0596PP.

[13] E.D. Bateman, S.S. Hurd, P.J. Barnes, J. Bousquet, J.M. Drazen, M. FitzGerald, et al., Global strategy for asthma management and prevention: GINA executive summary, Eur. Respir. J. 31 (2008) 143–178. http://dx.doi.org/10.1183/09031936.00138707.

[14] C.-E. Luyt, N. Bréchot, A. Combes, J.-L. Trouillet, J. Chastre, Delivering antibiotics to the lungs of patients with ventilator-associated pneumonia: an update, Expert Rev. Anti-Infect. Ther. 11 (2013) 511–521. http://dx.doi.org/10.1586/eri.13.36.

[15] A.S. Michalopoulos, Aerosolized antibiotics: the past, present and future, with a special emphasis on inhaled colistin, Expert Opin. Drug Deliv. 9 (2012) 493–495. http://dx.doi.org/10.1517/17425247.2012.676039.

[16] D. Lightwood, V. O'Dowd, B. Carrington, V. Veverka, M.D. Carr, M. Tservistas, et al., The discovery, engineering and characterisation of a highly potent anti-human IL-13 fab fragment designed for administration by inhalation, J. Mol. Biol. 425 (2013) 577–593. http://dx.doi.org/10.1016/j.jmb.2012.11.036.

[17] A. Maillet, L. Guilleminault, E. Lemarié, S. Lerondel, N. Azzopardi, J. Montharu, et al., The airways, a novel route for delivering monoclonal antibodies to treat lung tumors, Pharm. Res. 28 (2011) 2147–2156. http://dx.doi.org/10.1007/s11095-011-0442-5.

[18] J. Hill, J.E. Eyles, S.J. Elvin, G.D. Healey, R.A. Lukaszewski, R.W. Titball, Administration of antibody to the lung protects mice against pneumonic plague, Infect. Immun. 74 (2006) 3068–3070. http://dx.doi.org/10.1128/IAI. 74.5.3068-3070.2006.

[19] M.A. Poli, V.R. Rivera, M.L. Pitt, P. Vogel, Aerosolized specific antibody protects mice from lung injury associated with aerosolized ricin exposure, Toxicon 34 (1996) 1037–1044.

[20] J. Hacha, K. Tomlinson, L. Maertens, G. Paulissen, N. Rocks, J.-M. Foidart, et al., Nebulized anti-IL-13 monoclonal antibody Fab′ fragment reduces allergen-induced asthma, Am. J. Respir. Cell Mol. Biol. 47 (2012) 709–717. http://dx.doi.org/10.1165/rcmb.2012-0031OC.

[21] J.V. Fahy, D.W. Cockcroft, L.P. Boulet, H.H. Wong, F. Deschesnes, E.E. Davis, et al., Effect of aerosolized anti-IgE (E25) on airway responses to inhaled allergen in asthmatic subjects, Am. J. Respir. Crit. Care Med. 160 (1999) 1023–1027. http://dx.doi.org/10.1164/ajrccm.160.3.9810012.

[22] S. Holgate, T. Casale, S. Wenzel, J. Bousquet, Y. Deniz, C. Reisner, The anti-inflammatory effects of omalizumab confirm the central role of IgE in allergic

inflammation, J. Allergy Clin. Immunol. 115 (2005) 459–465. http://dx.doi.org/10.1016/j.jaci.2004.11.053.
[23] N.E. Simister, C.M. Story, Human placental Fc receptors and the transmission of antibodies from mother to fetus, J. Reprod. Immunol. 37 (1997) 1–23.
[24] K. Baker, S.-W. Qiao, T. Kuo, K. Kobayashi, M. Yoshida, W.I. Lencer, et al., Immune and non-immune functions of the (not so) neonatal Fc receptor, FcRn, Semin. Immunopathol. 31 (2009) 223–236. http://dx.doi.org/10.1007/s00281-009-0160-9.
[25] T.T. Kuo, K. Baker, M. Yoshida, S.-W. Qiao, V.G. Aveson, W.I. Lencer, et al., Neonatal Fc receptor: from immunity to therapeutics, J. Clin. Immunol. 30 (2010) 777–789. http://dx.doi.org/10.1007/s10875-010-9468-4.
[26] G.M. Spiekermann, P.W. Finn, E.S. Ward, J. Dumont, B.L. Dickinson, R.S. Blumberg, et al., Receptor-mediated immunoglobulin G transport across mucosal barriers in adult life: functional expression of FcRn in the mammalian lung, J. Exp. Med. 196 (2002) 303–310.
[27] A.J. Bitonti, J.A. Dumont, S.C. Low, R.T. Peters, K.E. Kropp, V.J. Palombella, et al., Pulmonary delivery of an erythropoietin Fc fusion protein in non-human primates through an immunoglobulin transport pathway, Proc. Natl. Acad. Sci. U. S. A. 101 (2004) 9763–9768. http://dx.doi.org/10.1073/pnas.0403235101.
[28] J.A. Dumont, A.J. Bitonti, D. Clark, S. Evans, M. Pickford, S.P. Newman, Delivery of an erythropoietin-Fc fusion protein by inhalation in humans through an immunoglobulin transport pathway, J. Aerosol Med. 18 (2005) 294–303. http://dx.doi.org/10.1089/jam.2005.18.294.
[29] M. Sakagami, Y. Omidi, L. Campbell, L.E. Kandalaft, C.J. Morris, J. Barar, et al., Expression and transport functionality of FcRn within rat alveolar epithelium: a study in primary cell culture and in the isolated perfused lung, Pharm. Res. 23 (2006) 270–279. http://dx.doi.org/10.1007/s11095-005-9226-0.
[30] P.M. Smith-Jones, D. Solit, F. Afroze, N. Rosen, S.M. Larson, Early tumor response to Hsp90 therapy using HER2 PET: comparison with 18F-FDG PET, J. Nucl. Med. 47 (2006) 793–796.
[31] S.E. Beck, B.L. Laube, C.I. Barberena, A.C. Fischer, R.J. Adams, K. Chesnut, et al., Deposition and expression of aerosolized rAAV vectors in the lungs of Rhesus macaques, Mol. Ther. 6 (2002) 546–554.
[32] N. Cézé, D. Ternant, F. Piller, D. Degenne, N. Azzopardi, E. Dorval, et al., An enzyme-linked immunosorbent assay for therapeutic drug monitoring of cetuximab, Ther. Drug Monit. 31 (2009) 597–601. http://dx.doi.org/10.1097/FTD.0b013e3181b33da3.
[33] R.J. Bauer, S. Guzy, C. Ng, A survey of population analysis methods and software for complex pharmacokinetic and pharmacodynamic models with examples, AAPS J. 9 (2007) E60–E83. http://dx.doi.org/10.1208/aapsj0901007.
[34] T. Jaki, M.J. Wolfsegger, Estimation of pharmacokinetic parameters with the R package PK, Pharm. Stat. 10 (2011) 284–288. http://dx.doi.org/10.1002/pst.449.
[35] R Core Team, R: A Language and Environment for Statistical Computing, R Foundation for Statistical Computing, Vienna, Austria, 2013. (URL http://www.R-project.org/).
[36] J. Mendelsohn, J. Baselga, Status of epidermal growth factor receptor antagonists in the biology and treatment of cancer, J. Clin. Oncol. 21 (2003) 2787–2799. http://dx.doi.org/10.1200/JCO.2003.01.504.
[37] N. Ledón, A. Casacó, E. Casanova, I. Beausoleil, Comparative analysis of binding affinities to epidermal growth factor receptor of monoclonal antibodies nimotuzumab and cetuximab using different experimental animal models, Placenta 32 (2011) 531–534. http://dx.doi.org/10.1016/j.placenta.2011.04.008.
[38] S. Lerondel, A. Le Pape, Bioluminescence imaging in rodents: when light illuminates cancer research, Curr. Mol. Imaging 2 (2013) 18–29. http://dx.doi.org/10.2174/2211555211302010004.
[39] A.J. Bitonti, J.A. Dumont, Pulmonary administration of therapeutic proteins using an immunoglobulin transport pathway, Adv. Drug Deliv. Rev. 58 (2006) 1106–1118. http://dx.doi.org/10.1016/j.addr.2006.07.015.
[40] K.-J. Kim, T.E. Fandy, V.H.L. Lee, D.K. Ann, Z. Borok, E.D. Crandall, Net absorption of IgG *via* FcRn-mediated transcytosis across rat alveolar epithelial cell monolayers, Am. J. Physiol. Lung Cell. Mol. Physiol. 287 (2004) L616–L622. http://dx.doi.org/10.1152/ajplung.00121.2004.
[41] D.W. Nicholson, A. Ali, N.A. Thornberry, J.P. Vaillancourt, C.K. Ding, M. Gallant, et al., Identification and inhibition of the ICE/CED-3 protease necessary for mammalian apoptosis, Nature 376 (1995) 37–43. http://dx.doi.org/10.1038/376037a0.
[42] X. Li, Y. Lu, T. Pan, Z. Fan, Roles of autophagy in cetuximab-mediated cancer therapy against EGFR, Autophagy 6 (2010) 1066–1077. http://dx.doi.org/10.4161/auto.6.8.13366.
[43] J.H.E. Baker, K.E. Lindquist, L.A. Huxham, A.H. Kyle, J.T. Sy, A.I. Minchinton, Direct visualization of heterogeneous extravascular distribution of trastuzumab in human epidermal growth factor receptor type 2 overexpressing xenografts, Clin. Cancer Res. 14 (2008) 2171–2179. http://dx.doi.org/10.1158/1078-0432.CCR-07-4465.
[44] D. Daydé, D. Ternant, M. Ohresser, S. Lerondel, S. Pesnel, H. Watier, et al., Tumor burden influences exposure and response to rituximab: pharmacokinetic-pharmacodynamic modeling using a syngeneic bioluminescent murine model expressing human CD20, Blood 113 (2009) 3765–3772. http://dx.doi.org/10.1182/blood-2008-08-175125.
[45] C.M. Lee, I.F. Tannock, The distribution of the therapeutic monoclonal antibodies cetuximab and trastuzumab within solid tumors, BMC Cancer 10 (2010) 255. http://dx.doi.org/10.1186/1471-2407-10-255.
[46] S.I. Rudnick, J. Lou, C.C. Shaller, Y. Tang, A.J.P. Klein-Szanto, L.M. Weiner, et al., Influence of affinity and antigen internalization on the uptake and penetration of Anti-HER2 antibodies in solid tumors, Cancer Res. 71 (2011) 2250–2259. http://dx.doi.org/10.1158/0008-5472.CAN-10-2277.
[47] J.S. Patton, Mechanisms of macromolecule absorption by the lungs, Adv. Drug Deliv. Rev. 19 (1996) 3–36. http://dx.doi.org/10.1016/0169-409X(95)00113-L.
[48] J.S. Patton, C.S. Fishburn, J.G. Weers, The lungs as a portal of entry for systemic drug delivery, Proc. Am. Thorac. Soc. 1 (2004) 338–344. http://dx.doi.org/10.1513/pats.200409-049TA.
[49] J.S. Patton, P.R. Byron, Inhaling medicines: delivering drugs to the body through the lungs, Nat. Rev. Drug Discov. 6 (2007) 67–74. http://dx.doi.org/10.1038/nrd2153.
[50] C. Kliwinski, P.R. Cooper, R. Perkinson, J.R. Mabus, S.H. Tam, T.M. Wilkinson, et al., Contribution of FcRn binding to intestinal uptake of IgG in suckling rat pups and human FcRn-transgenic mice, Am. J. Physiol. Gastrointest. Liver Physiol. 304 (2013) G262–G270. http://dx.doi.org/10.1152/ajpgi.00340.2012.
[51] N. Azzopardi, T. Lecomte, D. Ternant, M. Boisdron-Celle, F. Piller, A. Morel, et al., Cetuximab pharmacokinetics influences progression-free survival of metastatic colorectal cancer patients, Clin. Cancer Res. 17 (2011) 6329–6337. http://dx.doi.org/10.1158/1078-0432.CCR-11-1081.
[52] S.A. Antoniu, Monoclonal antibodies for asthma and chronic obstructive pulmonary disease, Expert. Opin. Biol. Ther. 13 (2013) 257–268. http://dx.doi.org/10.1517/14712598.2012.758247.
[53] R. Rafii, M.M. Juarez, T.E. Albertson, A.L. Chan, A review of current and novel therapies for idiopathic pulmonary fibrosis, J. Thorac. Dis. 5 (2013) 48–73. http://dx.doi.org/10.3978/j.issn. 2072-1439.2012.12.07.
[54] Jitendra, P.K. Sharma, S. Bansal, A. Banik, Noninvasive routes of proteins and peptides drug delivery, Indian J. Pharm. Sci 73 (2011) 367–375. http://dx.doi.org/10.4103/0250-474X.95608.
[55] S. Wenzel, D. Wilbraham, R. Fuller, E.B. Getz, M. Longphre, Effect of an interleukin-4 variant on late phase asthmatic response to allergen challenge in asthmatic patients: results of two phase 2a studies, Lancet 370 (2007) 1422–1431. http://dx.doi.org/10.1016/S0140-6736(07)61600-6.
[56] N. Roche, T. Chinet, G. Huchon, Ambulatory inhalation therapy in obstructive lung diseases, Respiration 64 (1997) 121–130.